Industrial Chemistry & Materials

Accepted Manuscript

This article can be cited before page numbers have been issued, to do this please use: W. Zhang, Y. Li, Y. He, S. Zhang, H. Li, H. Zheng and Q. Zhu, *Ind. Chem. Mater.*, 2024, DOI: 10.1039/D4IM00067F.

View Article Online
DOI: 10.1039/D4IM00067F

ARTICLE

Membrane-free sequential paired electrosynthesis of 1,4-hydroquinone from phenol over a self-supported electrocatalytic electrode

Received 00th January 20xx,
Accepted 00th January 20xx

DOI: 10.1039/x0xx00000x

Wei-Ling Zhang,[abc] Ya-Jing Li,[ab] Yingchun He,[b] Shao Zhang,*[b] Haohong Li,[ac] Huidong Zheng*[ac] and Qi-Long Zhu*[bd]

The sequential paired electrosynthesis capable of the production of organic chemicals through a series of electrochemical reactions that occur consecutively and in pairs are of high significance. Herein, a three-dimensional porous carbon felt-loaded PbO_2 electrode (PbO_2/CF) with a self-supported nanostructure was fabricated using a double-cathode electrodeposition method, which severed as an efficient electrocatalyst enabling the unique sequential paired electrosynthesis of 1,4-hydroquinone (1,4-HQ) from phenol in a membrane-free electrolytic cell. In such exotic paired electrolysis system, phenol is first oxidized to *p*-benzoquinone at the anode, which is subsequently reduced to 1,4-HQ at the cathode. The as-obtained PbO_2/CF electrode exhibited a remarkable electrochemical performance, achieving impressive conversion and selectivity of 94.5% and 72.1%, respectively, for the conversion of phenol to 1,4-HQ. This exceptional performance can be attributed to the open porous self-supported structure of the PbO_2/CF electrode, which improves the active site exposure and substrate adsorption capability and reduces mass and charge transfer resistance. Furthermore, the catalyst electrode well maintained its structure integrity even after 140 hours of long-term use, further highlighting its promising application for the electrosynthesis of 1,4-HQ. Moreover, this sequential paired electrosynthesis strategy can be further extended to other substrates with electron-withdrawing/donating groups over the PbO_2/CF electrode. The proof of concept in this innovative sequential paired electrosynthesis could provide a sustainable and efficient way to produce various desired organic compounds.

Keywords: Phenol; 1,4-Hydroquinone; Electrocatalysis; Sequential paired electrosynthesis; Self-supported electrodes

1 Introduction

1,4-Hydroquinone (1,4-HQ) and its derivatives have great industrial importance as they serve as raw materials and intermediates in the synthesis of various fine chemicals including photographic film developers, dyes, antioxidations, and polymer materials.[1–3] In the past, 1,4-HQ was mainly synthesized by aniline,[4] and diisopropyl benzene via classical chemical methods.[5] However, these methods usually suffer from several disadvantages, involving low production efficiency, long reaction routes, high consumption of raw materials, and serious environmental pollution, which limit the further development.[5,6] Subsequently, one-step hydroxylation of phenol has received great attention. However, the hydroxylation of phenol is commonly carried out by conventional thermochemical methods utilizing hydrogen peroxide (H_2O_2) as the oxidant,[7–9] which increases the cost and operational risk. Most importantly, the efficient and para-selective hydroxylation of the phenolic C-H bond is a challenging problem under the reaction conditions and the selectivity of reported methods has not been satisfactory.[10–12] Generally, catechol, a byproduct that has relatively few industrial applications, is more easily obtained utilizing thermal catalysis. Thus, the efficient processes for green and selective synthesis of 1,4-HQ are still highly desired.

Electrosynthesis using water as the oxidant is a sustainable, safe, and eco-friendly strategy that facilitates chemical synthesis at ambient temperature and pressure.[13–16] Up to now, there has been some research into the electrooxidation of phenol.[17,18] Yet, the majority of previous studies have focused on the oxidative degradation of phenol.[19–22] Likewise, some researchers have studied the influence of pH, temperature, and concentration on the electrooxidation of phenol on Pt electrode.[23,24] However, there are only a very limited number of investigations on the production of high value-added products. For example, in acidic electrolytes, Baravkar et al.[25] demonstrated that surface-modified reticulated glassy carbon (RVC) based electrodes can be utilized for the electrooxidation of phenol, introducing functional groups like -C-O, -C=O, and -

[a] College of Chemical Engineering and College of Chemistry, Fuzhou University, Fuzhou 350108, China.
[b] State Key Laboratory of Structural Chemistry, Fujian Institute of Research on the Structure of Matter, Chinese Academy of Sciences (CAS), Fuzhou 350002, China.
[c] Qingyuan Innovation Laboratory, Quanzhou 362801, China.
[d] School of Materials Science and Engineering, Zhejiang Sci-Tech University, Hangzhou 310018, China.
E-mail: zhangshao@fjirsm.ac.cn, youngman@fzu.edu.cn and qlzhu@fjirsm.ac.cn
† Supplementary Information available. See DOI: 10.1039/x0xx00000x

COO, which showed resistance to surface poisoning and provided good product selectivity. Although the selectivity for 1,4-HQ can reach up to 87%, the fast reaction rate required the additive oxidant (H_2O_2) to the electrolyte. Besides, the low mechanical strength in flow cell is a disadvantage of the RVC electrodes.[26] Meanwhile, Li et al.[27] prepared the NiV-layered double hydroxide nanosheets (NiV-LDH-NS) with enriched defects and bimetallic synergistic effects for electrochemical phenol hydroxylation under alkaline conditions, confirming that electron-rich defects accelerated the V^{4+}/V^{5+} redox to produce hydroxyl radicals (·OH) involved in the electrochemical phenol hydroxylation. Despite these progresses, it is still a challenge to prepare catalytic electrodes for efficient electrochemical production of 1,4-HQ from phenol in an aqueous electrolyte simultaneously with good selectivity and long-term stability.

Recently, researchers have conducted the explorations of paired electrosynthesis to produce various desired compounds through a series of electrochemical reactions that occur in pairs,[28–32] including the production of 1,4-HQ.[33,34] Specially, the sequential paired electrosynthesis, where multiple electrochemical reactions occur in sequence to yield a single product, involves the coupling of both oxidation and reduction reactions and allows for the synthesis of desired compounds in a controlled and efficient manner.[35] For instance, Muchez and colleagues[36] reported an innovative electrochemical procedure for synthesizing α-hydroxy acids from aromatic alcohols, which encompasses a two-step reaction within an undivided electrochemical cell. Initially, in the presence of a small amount of water, aromatic alcohols are efficiently oxidized to ketones or aldehydes at the anode, and then converted to α-hydroxy acids by coupling with CO_2 at the cathode, achieving yields of up to 61%. Inspired by these unique merits, we proposed a sequential paired electrosynthesis strategy for electrochemically converting phenol to 1,4-HQ, which entails the electrochemical redox processes involving the oxidation of phenol to *p*-benzoquinone at the anode, followed by the subsequent reduction to 1,4-HQ at the cathode. Since *p*-benzoquinone is readily to be selectively reduced into 1,4-HQ, the selective electrooxidation of phenol to *p*-benzoquinone at the anode is a critical step, which, however, still suffers from insufficient activity and selectivity of the electrocatalysts. Research has been indicated that the electrode surface is highly susceptible to formation of non-conductive polymers during electrooxidation of phenol.[37,38] Thus, the design of the efficient anode electrode is a key to the sequential paired electrosynthesis of 1,4-HQ from phenol. PbO_2 electrocatalysts are low-cost and readily to prepare, and their significantly high electrical conductivity and chemical stability make them one of the most promising anode materials for electrocatalytic applications.[39–41]

Based on the above considerations, in this work, the self-supported PbO_2/CF anode was facilely obtained through the simple double-cathode electrodeposition method, which was subsequently applied as an efficient electrocatalyst for the membrane-free sequential paired electrosynthesis of 1,4-HQ from phenol (Scheme 1). The as-obtained PbO_2/CF anode displayed exceptional electrochemical performance with high activity and selectivity for 1,4-HQ production in this system, which can be attributed to the open porous self-supported nanostructure of PbO_2/CF and the efficient sequential paired electrolysis configuration. Additionally, the long lifespan of the PbO_2/CF electrode and its capacity to oxidize a series of phenol derivatives make such sequential paired electrosynthesis strategy a potential approach for producing value-added compounds.

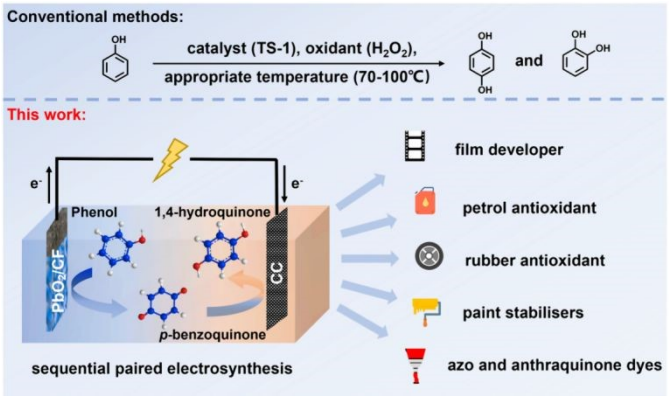

Scheme 1 The traditional synthesis and schematic of membrane-free sequential paired electrosynthesis of 1,4-HQ from phenol over PbO_2/CF and CC (Note: TS-1 = titanosilicate-1).

2 Results and discussion

2.1 Characteristics of the PbO_2/CF electrode

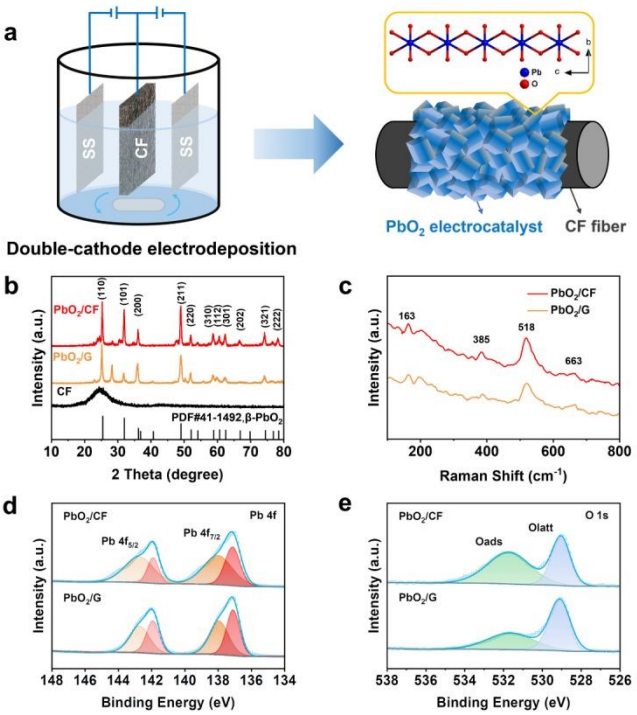

Fig. 1 (a) Scheme illustration of the double-cathode electrodeposited method for the synthesis of PbO_2/CF and the growth of loaded PbO_2; (b) XRD patterns of PbO_2/CF, PbO_2/G and CF substrate with PDF card of β-PbO_2; (c) Raman spectra of PbO_2/CF and PbO_2/G; XPS spectra of (d) Pb 4f and (e) O 1s of PbO_2/CF and PbO_2/G.

As shown in Fig.1a, the self-supported PbO_2/CF electrode was prepared via a facile one-step double-cathode

View Article Online
DOI: 10.1039/D4IM00067F

electrodeposition method. According to Fig. 1b, in the XRD spectrum of the CF substrate, a distinct diffraction peak appears at 2θ = 25.1° assigned to graphitic carbon, while a broad peak shows the presence of amorphous carbon in CF. In the XRD spectra of PbO_2/CF and PbO_2/G, the CF broad peak is almost completely concealed by those of the PbO_2 phase, which indicates high crystallinity and compactness of PbO_2 on the electrode. The strong peaks at 25.4°, 32°, 36.2°, and 49° are attributed to the presence of (110), (101), (200), and (211) planes of β-PbO_2 (JCPDS No. 41-1492), respectively. Nonetheless, the two very weak peaks at 23.3° and 28.6° are related to α-PbO_2 (JCPDS No. 45-1416). The sharp diffraction peaks of β-PbO_2 suggest that it is the main phase. The Raman spectra of the PbO_2/CF and PbO_2/G samples show the same peaks at 163, 385, 518, and 663 cm^{-1}, which are attributed to the feature of β-PbO_2 (Fig. 1c).[42,43] The XPS survey spectra (Fig. S1) demonstrate that both PbO_2/CF and PbO_2/G contain only Pb and O elements. Accordingly, the detailed electronic structures of Pb 4f and O 1s spectra are presented in Fig. 1d-e. The typical XPS peaks of Pb 4f (Fig. 1d) with binding energies at 137.2 and 138.3 eV are assigned to Pb $4f_{7/2}$, and the peaks at 142 and 142.9 eV are identified as Pb $4f_{5/2}$.[44] Meanwhile, the O 1s peak (Fig. 1e) can be matched with two peaks at 529.8 and 531.6 eV, which are associated with the Pb-O and O-H groups, respectively.[45] These results confirmed that the β-PbO_2 phase has been successfully deposited onto the surface of carbon felt.

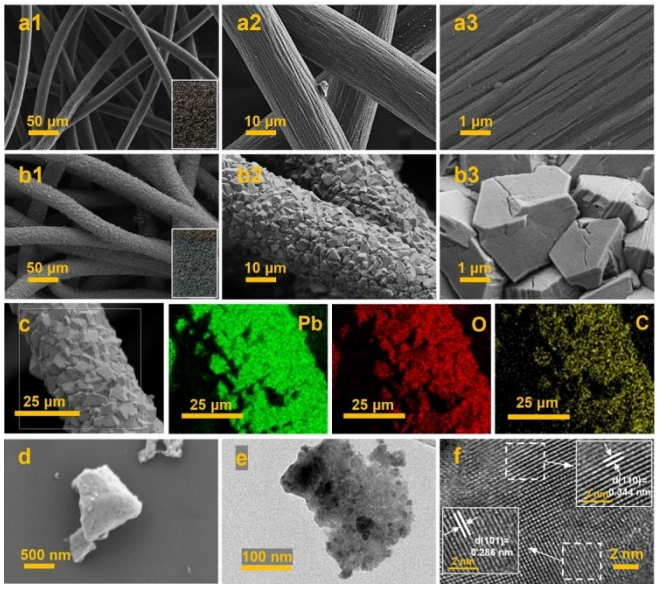

Fig. 2 SEM images of (a1-a3) bare CF substrate and (b1-b3) PbO_2/CF; (c) EDX elemental mapping images of PbO_2/CF; (d) SEM, (e) TEM, and (f) HRTEM images of the PbO_2 nanocrystals stripped from PbO_2/CF.

The surface morphology of the CF substrate is presented in Fig. 2a1-a3, showing that the bare CF substrate is composed of a three-dimensional network of long cylindrical fibers with rough grooves, which is beneficial for the adhesion of Pb^{2+} to the substrate with a strong bonding effect. According to Fig. 2b1-b3, after the PbO_2 electrodeposition, all the carbon fibers are uniformly and completely coated by the PbO_2 nanocrystals without any crack in the form of pyramidal particles. Also, as observed in the inset of Fig. 2b1, the surface-modified CF reveals a noticeable color change from black to grey. The porous structure of PbO_2/CF displays a higher active surface area which could enhance the mass transfer in comparison with the 2D PbO_2/G electrode (Fig. S2). The EDX mapping and spectra images of PbO_2/CF are presented in Fig. 2c and Fig. S3a, respectively. It can be seen that lead (Pb) and oxygen (O) elements are uniformly distributed on the CF. Fig. 2d-e further show the morphology of the PbO_2 nanocrystal stripped from PbO_2/CF, verifying the nanocrystal nature of PbO_2. In Fig. 2f, the lattice fringes of 0.344 and 0.285 nm are identified in the high-resolution TEM (HRTEM) image, corresponding well with the (110) and (101) lattice planes of β-PbO_2, which is consistent with the XRD analysis result.

2.2 Electrochemical characterization of the PbO_2/CF electrode

The cyclic voltammetry (CV) analyses were conducted in a three-electrode system. In Fig. S4, the oxidation and reduction of phenol on the PbO_2/CF and PbO_2/G anodes were tested in 0.1 M H_2SO_4 with or without the presence of 20 mM phenol. In the acidic aqueous electrolyte, phenol molecules can be adsorbed onto the PbO_2 electrode surface and oxidized by losing one electron and proton to form phenoxy radical. The intermediate species can be activated on the electrode surface to efficiently react with water to form the *o*- or *p*-benzoquinone. As illustrated in Fig. S4a, a stronger adsorption oxidation peak is visible at 1.59 V (vs. Ag/AgCl) over PbO_2/CF compared to that of PbO_2/G (Fig. S4b), which confirms that the 3D self-supported electrode has a higher electrochemical activity.[46] The transfer kinetics of electrons between the electrode and electrolyte was analyzed through electrochemical impedance spectroscopy (EIS). Fig. S5 shows that PbO_2/CF exhibits a lower ohmic resistance (R_s) compared to PbO_2/G (6.66 vs. 9.75 Ω), suggesting that PbO_2/CF has higher conductivity, leading to the enhanced electrochemical performance. Additionally, PbO_2/CF presents faster interfacial charge transfer kinetics during the electrochemical process, as evidenced by a lower charge transfer resistance (R_{ct}) in contrast to PbO_2/G (32.37 vs. 592.7 Ω). Meanwhile, owing to the 3D self-supported structure, the PbO_2/CF electrode offers a larger surface area and exposes more active sites compared to PbO_2/G. This observation is in line with the analysis of the porous nanostructure and the electrochemical activity of the PbO_2/CF electrode.

2.3 Electrocatalytic performance for sequential paired electrosynthesis of 1,4-HQ from phenol

The electrosynthesis of 1,4-HQ from phenol was conducted via the sequential paired electrosynthesis system with PbO_2/CF and carbon cloth as the anode and cathode, respectively, in a membrane-free two-electrode electrolysis cell under a galvanostatic mode. Through this unique paired electrosynthesis, phenol is first selectively oxidized to *p*-benzoquinone at the anode, which is subsequently reduced to 1,4-HQ at the cathode. Since the second-step reduction of *p*-benzoquinone to 1,4-HQ at the cathode is relatively readily and selective, the selective oxidation of phenol to *p*-benzoquinone and the avoidance of excessive oxidation at the anode are

View Article Online
DOI: 10.1039/D4IM00067F

decisive. The concentrations of reactants and products were quantitatively evaluated via nuclear magnetic resonance (NMR) spectroscopy (Fig. S6). The electrolysis of phenol to 1,4-HQ was first studied at various current densities ranging from 5 to 20 mA cm^{-2}, with an applied charge of 290 C. The results shown in Fig. 3a and 3b were obtained, when PbO_2/CF and PbO_2/G were respectively used as the anodes. As depicted in Fig. 3a, it is evident that the electrosynthesis with the PbO_2/G electrode yielded small amounts of 1,4-HQ product. By contrast, the yield of 1,4-HQ was significantly improved to 68.2% at 10 mA cm^{-2}, with Faradaic efficiency (FE) of 55% and small amount of by-products, when the reaction was carried out with the PbO_2/CF electrode (Fig. 3b). Furthermore, the conversion of phenol at a given charge condition remained above 90% upon increasing the applied current density, whereas the selectivity for 1,4-HQ was initially rosed but later declined, indicating that higher current densities are more prone to favor the undesired side reactions, resulting in a decrease in the desired product quantity. This could be attributed to the fact that, at the higher current densities, the phenol substrate was quickly oxidized at the anode without adequate time for the intermediates to leave the electrode before further oxidation occurrence. Based on the results, the current density of 10 mA cm^{-2} achieves the highest selectivity and thus was applied for further study. In addition, the optimization of sulfuric acid concentration in the electrolyte solution was performed (Fig. S7a) within a measured range from 0.1 to 1 M. As the acid concentration increased, the selectivity of the desired 1,4-HQ product decreased. This phenomenon can be ascribed to the heightened susceptibility of the cathode to competing HER in the solution with elevated acid concentration. Furthermore, the *p*-benzoquinone generated by anodic oxidation was not promptly reduced at the cathode, resulting in further oxidation and corresponding a decrease in the yield of the 1,4-HQ product. The optimization of amount of the charge was also performed (Fig. S7b). It was observed that applying a charge of 290 C at a constant current density of 10 mA cm^{-2} yielded the highest selectivity for 1,4-HQ, with a concentration of approximately 13.6 mM. Therefore, according to the optimal reaction conditions, the electrosynthesis was conducted in 0.1 M H_2SO_4 solution at the current density of 10 mA cm^{-2} under the charge of 290 C. When compared to other chemical methods (Table S1), such electrosynthesis method demonstrated here delivers much superior conversion and selectivity towards 1,4-HQ under mild reaction conditions.

The trends in substrate conversion rate are shown in Fig. 3c, with a gradual decrease from 0.8 to 0.6 mmol L^{-1} h^{-1} at the PbO_2/CF electrode. This may be due to the rapid consumption of the substrate and subsequent decrease in phenol concentration during electrolysis, resulting in a decline in the reaction rate. On the other hand, the conversion rate at the PbO_2/G electrode was around 0.28 mmol L^{-1} h^{-1}, much lower than that at the PbO_2/CF electrode. The generation rate of 1,4-HQ product is displayed in Fig. 3d, with the PbO_2/CF electrode exhibiting a rate almost twice as high as that of the PbO_2/G electrode. The long-term galvanostatic tests of the PbO_2/CF and PbO_2/G electrodes were further investigated at the current density of 10 mA cm^{-2} with 45 mM phenol in 0.1 M H_2SO_4 electrolyte solution (Fig. 3e, S8). As time progressed, the actual electrode potential remained steady at around 3.0 V. The PbO_2/CF anode exhibited a 1,4-HQ yield of 55% after 60 hours, while the PbO_2/G anode only showed 28%, half that of PbO_2/CF. More visually, the product generation kinetics constant (k) for PbO_2/CF (0.999 h^{-1}) was 2.45 times higher than that for PbO_2/G (0.408 h^{-1}) under the same conditions (Fig. S9). Satisfyingly, the service life of the PbO_2/CF anode is longer than 144 hours, demonstrating excellent durability in the reactions. This remarkable stability was further confirmed by characterizing the recycled electrode with XRD and SEM techniques, which indicate that the crystalline structure of PbO_2 in the electrode was well-preserved (Fig. S10a). The SEM images (Fig. S10c) show that the PbO_2/CF electrode still had a compact and uniform structure after long-term use. However, slight decomposition of the PbO_2/G electrode was observed during the reaction process, as evidenced in Fig. S11. Additionally, the CF substrate was found to be unsuitable for use as the anode electrode (Fig. S12). In comparison to the 2D PbO_2/G, the 3D structure of the PbO_2/CF electrode offers a larger catalytic surface and more active sites, which could be the main factors for its remarkable performance for 1,4-HQ production.

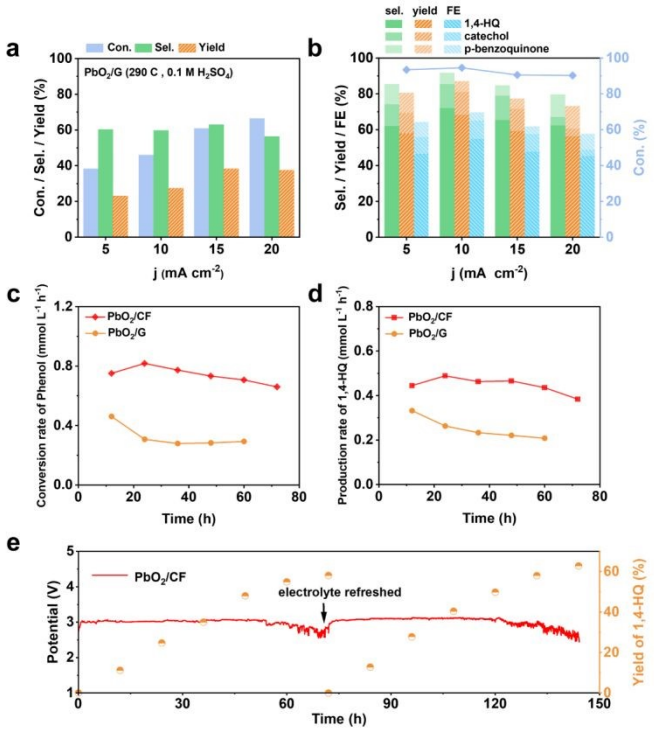

Fig. 3 (a) phenol conversion, 1,4-HQ selectivity and yields at various current densities in 0.1 M H_2SO_4 with an applied charge of 290 C over PbO_2/G; (b) phenol conversion, product selectivity, yields, and FEs at various current densities in 0.1 M H_2SO_4 with an applied charge of 290 C over PbO_2/CF; (c) phenol conversion rates and (d) 1,4-HQ production rates over PbO_2/CF and PbO_2/G; (e) long-term stability test of PbO_2/CF with 45 mM phenol in 0.1 M H_2SO_4 solution (75 mL) at 10 mA cm^{-2}.

2.4 Reaction mechanisms for sequential paired electrosynthesis of 1,4-HQ from phenol

To better insight into the reaction mechanisms, the pathways of the sequential paired electrosynthesis of 1,4-HQ from phenol in the membrane-free electrolysis system were further

View Article Online
DOI: 10.1039/D4IM00067F

investigated. Based on previous research on the electrochemical conversion mechanisms of phenol to various products in an undivided cell, the possible involved reactions are shown in Scheme S1.[47,48] During the electrolysis process, phenol is oxidized on the anode, resulting in the formation of three types of phenoxy radical.[49] Extensive research has documented that the radical situated at the para position is comparatively more stable than the radical located *ortho* to the carbonyl, and the former can undergo hydration to yield *p*-benzoquinone, while the latter can be hydrated to form *o*-benzoquinone.[50] Therefore, it is probable that the electrooxidation of phenol is more likely to produce the intermediate of *p*-benzoquinone, which subsequently receive electrons and protons to become 1,4-HQ at the cathode.

To verify the fact that the actual reactions follow the established pathways, diverse electrolysis configurations were set up to study the reaction pathways and ^{1}H NMR was used to analyze the products (Fig. 4). In an undivided cell, the sequential paired electrolysis of phenol occurred, and the predominant outcome was manifested to be 1,4-HQ (Fig. 4a,b). Subsequently, comparative reactions were conducted in an H-type cell with the membrane separator, where *p*-benzoquinone was the predominant anodic product when phenol was used as the substrate (Fig. 4c, 4d). On the other hand, 1,4-HQ was the exclusive cathodic product when *p*-benzoquinone was used as the substrate (Fig. 4e, 4f). Furthermore, the conversion, selectivity, yield, and current efficiency were quantified (Fig. S13). These results certainly endorse that the reaction pathways

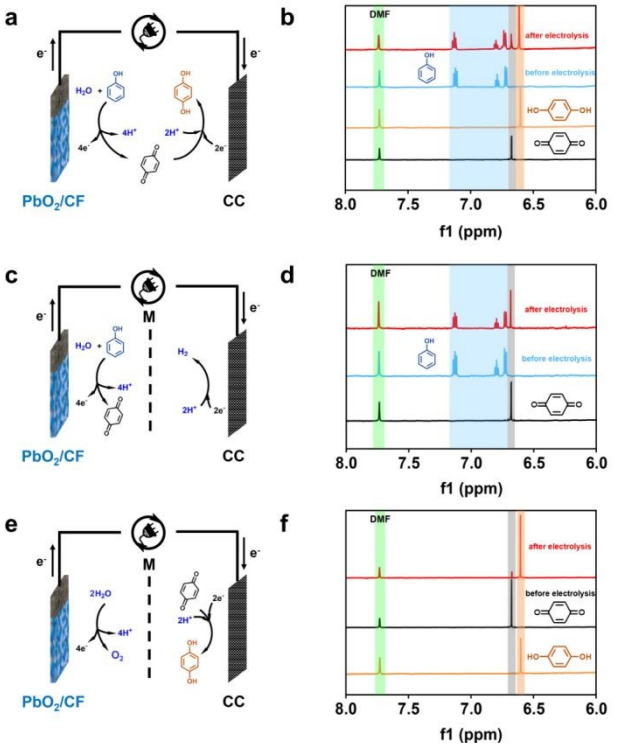

Fig. 4 Reaction pathways in diverse electrolysis configurations and corresponding ^{1}H NMR spectra of substrates and products. (a, b) membrane-free sequential paired electrosynthesis of 1,4-HQ from phenol; (c, d) membrane-separated phenol oxidation reaction coupling with HER (e, f) membrane-separated p-benzoquinone reduction reaction coupling with OER.

in such membrane-free sequential paired electrosynthesis follow the oxidation of phenol to *p*-benzoquinone and then the reduction to 1,4-HQ.

2.5 Substrate extension through sequential paired electrosynthesis

Finally, in order to gain a better understanding of the compatibility of this paired electrosynthesis strategy, our study was expanded to include other phenolic compounds under the same conditions (Table 1 and Fig. S14-16). The reactivity of phenols with electron-donating alkyl substitutions, such as *ortho*, *dimethyl*, and *trimethyl* cresols, was tested. It was observed that nearly all of the substrates exhibited the conversion exceeding 90%, with the exception of 2b. Additionally, we also screened the influence of the electro-withdrawing groups in phenols (e.g., *ortho*-chlorophenol and *ortho*-fluorophenol) on their reactivity, noting minimal variance in conversion ratio. However, an increase in electron-donating groups diminishes product selectivity, this phenomenon can be attributed to the spatial site-barrier effect caused by the increase in the number of methyl groups. This resulted in lower final yields, with the *ortho* isomer being the most productive, yielding 42.7% of 2b and 38.5% of 2c. The yield of 2d, which contains the highest number of methyl groups, is the lowest at 16.2%. Among substrates with electron-withdrawing groups, we noted a difference in product selectivity between 2-chlorophenol and 2-fluorophenol, likely due to the stronger ortho-para localization effect of the -F over the -Cl group. Specifically, *ortho*-chlorophenol afforded a higher yield of 40.1% for 2e, compared to *ortho*-fluorophenol's product 26.8% (2f). The results from our substrate scope analysis indicate that the phenols with few electron-donating groups or weaker electron-withdrawing groups tend to yield higher amounts of the corresponding 1,4-HQ derivatives (Fig. 5).

Table 1 Substrate extension through sequential paired electrosynthesis.[a] Molecular structures of the desired phenolic compounds and corresponding conversion, selectivity and yields.

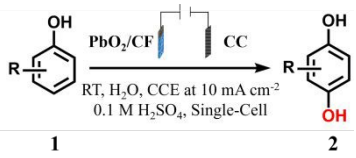

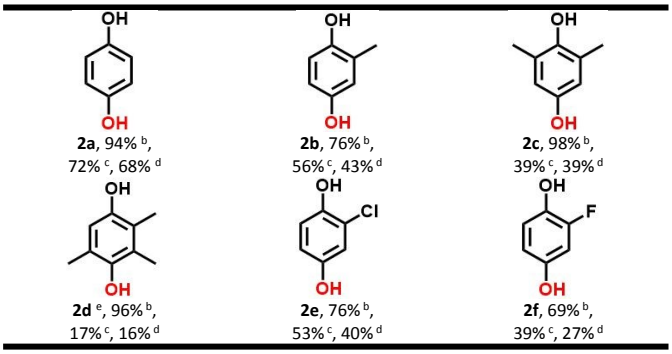

[a] The reaction conditions: primary phenols (20 mM); 30 mL of 0.1 M H_2SO_4 as the electrolyte; constant current of 10 mA cm^{-2} at room temperature; applied charge of 290 C; PbO_2/CF electrode and carbon cloth as the anode and cathode, respectively. The products were determined by GC analysis. [b] conversion (%); [c] selectivity (%); [d] yield (%); [e] the electrolyte solution (0.1 M H_2SO_4 in H_2O/MeCN (v:v = 24:6)).

View Article Online
DOI: 10.1039/D4IM00067F

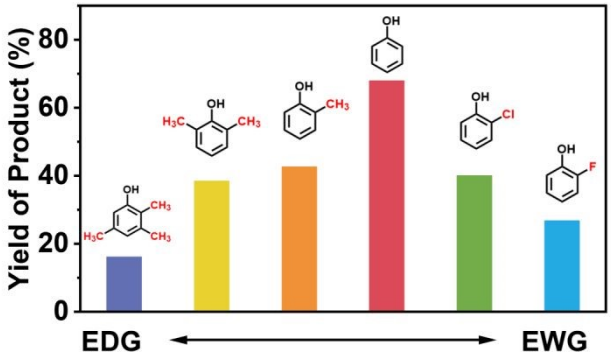

Fig. 5 Yield distribution of phenols with different functional groups.

3 Conclusion

In summary, a three-dimensional PbO_2/CF electrode was prepared using a facile one-step double-cathode electrodeposition method, which can serve as an efficient anodic electrocatalyst for the membrane-free sequential paired electrosynthesis of 1,4-HQ from phenol in an acidic electrolyte. The PbO_2/CF electrode, with its 3D porous structure, exhibits a high catalytic surface to sufficiently expose the active sites, improving the charge and mass transfer and enhancing the activity. Consequently, the PbO_2/CF electrode achieved the boosted catalytic performance for the sequential paired electrosynthesis with a phenol conversion of 94.5% and a 1,4-HQ selectivity of 72.1%, greatly surpassing the performance of the 2D PbO_2/G counterpart. Meanwhile, the efficiency of the PbO_2/CF electrode was well maintained for over 140 hours. Furthermore, the studies on the reaction pathways of this unique sequential paired electrosynthesis were well conducted. We also evaluated the compatibility of this electrosynthesis method with electro-withdrawing/donating phenols using the PbO_2/CF electrode. In conclusion, this study demonstrates the high potentials of the self-supporting electrocatalytic electrodes and the sequential paired electrosynthesis strategy for producing value-added chemical compounds.

4 Experiment

4.1 Electrode preparation

PbO_2/CF electrodes were prepared using a facile one-step double-cathode electrodeposited method. Typically,[51] the carbon felt (CF) was firstly cleaned by ultrasonicating sequentially in deionized water, 40% NaOH solution, and HNO_3/H_2SO_4 (v/v=3:1) aqueous solution for 30 min to increase surface oxygen functional groups. The cleaned CF substrate was rinsed several times with deionized water and anhydrous alcohol, and then dried in an oven at 60 °C. In a typical synthesis procedure, 12 mmol of Pb $(NO_3)_2$ and 6 mmol of HNO_3 were dissolved in 60 mL of deionized water. The resulting solution was then transferred into a single-compartment electrochemical cell that was equipped with three electrodes, all possessing identical dimensions. The cleaned CF sheet (2 cm × 3 cm) serving as the anode was positioned between two stainless steel (SS) meshes, with a separation distance of 1.5 cm. The electrodeposition was carried out at a constant current density of 60 mA cm^{-2} for 60 min at room temperature. The as-deposited PbO_2/CF was rinsed with deionized water several times and dried in an oven at 60 °C. As a comparison, the PbO_2/G electrode was prepared using the same electrodeposition method. For pre-treatment of graphite substrate, the surface was first sanded with emery paper and cleaned with 40% NaOH solution and HNO_3/H_2SO_4 mixture. Electrodeposition on the graphite was performed at a current density of 20 mA cm^{-2} for 120 min.

4.2 Electrode characterization

X-ray diffraction (XRD) patterns were collected on Rigaku Miniflex 600 X-ray diffractometer with Cu Kα radiation. The morphology and element distribution of the samples were obtained on a ZEISS SIGMA 300 field emission scanning electron microscope (SEM) and FEI Tecnai F20 transmission electron microscope (TEM). X-ray photoelectron spectroscopy (XPS) was examined using Thermo Fisher ESCALAB 250Xi with C 1s peak (binding energy = 284.8 eV) as the internal standard. The Raman spectra were acquired by Horiba Jobin Yvon LabRAM HR Raman spectrometer equipped with a 25 mW 633 nm laser. ^{1}H NMR spectra were recorded on the ECZ600S spectrometer (600 MHz).

4.3 Electrochemical experiments and analytical methods

All the electrochemical characterizations were performed with a CHI660E electrochemical workstation in an undivided cell with a three-electrode set-up. The as-prepared porous electrode (1.0×1.0 cm^2) and carbon cloth (CC) (1.0×1.0 cm^2) were used as the anode electrode (WE) and cathode electrode (CE), respectively. The Ag/AgCl (saturated KCl) was used as the reference electrode (RE). Cyclic voltammetry (CV) scans were recorded at a scan rate of 100 mV s^{-1}. The electrochemical impedance spectroscopy (EIS) was recorded with a frequency ranging from 0.01 to 105 Hz at the AC amplitude of 5 mV. All paired electrosynthesis measurements were performed using a two-electrode system in an undivided cell under constant current mode. The typical electrolyte contains 30 mL of 0.1 M H_2SO_4 aqueous solution with 20 mM phenol. After electrolysis, the liquid products were detected using ^{1}H nuclear magnetic resonance (NMR) with DMF serving as the internal standard or extracted by ethyl acetate and quantitatively analyzed by gas chromatography (GC, Shimadzu 2010 with an HP-5 column and an FID detector). The conversion of phenol (X) and the selectivity of its products (S) were calculated by the following equations, respectively.

$$X = \frac{n^0_{phenol} - n_{phenol}}{n^0_{phenol}} \times 100\%$$

$$S = \frac{n_M}{n^0_{phenol} - n_{phenol}} \times 100\%$$

where $n^0_{phenol}$is the initial phenol concentration, n_{phenol} and n_M are the concentration of phenol and 1,4-HQ, catechol, p-benzoquinone after electrolysis, respectively.

DOI: 10.1039/D4IM00067F

Faradaic efficiency (*FE*) was calculated according to the following expression:

$$FE = \frac{nzF}{Q} \times 100\%$$

where *n* is the amount of target product (moles), *z* is the number of electrons transferred to produce a target product molecule (*z* = 4 for p-benquinone; 2 for 1,4-HQ and catechol), *F* is Faraday constant (96485 C mol^{-1}), and Q is the total applied charge.

Author contributions

Wei-Ling Zhang: data curation, investigation, writing – original draft, writing – review & editing. Ya-Jing Li: investigation, validation. Yingchun He: resources, data curation. Shao Zhang: data curation, writing – review & editing. Haohong Li: project administration. Huidong Zheng: funding acquisition, resources methodology, supervision. Qi-Long Zhu: writing – review & editing, validation, supervision.

Conflicts of interest

There are no conflicts to declare.

Data availability

Data will be made available on request.

Acknowledgements

This work was supported by the National Natural Science Foundation of China (NSFC) (22175174, 22078065 and 52332007), the Natural Science Foundation of Fujian Province (2021J06033 and 2022L3092) and the Key Program of Qingyuan Innovation Laboratory (00221001).

References

1 X. Zhao, Z. Sun, Z. Zhu, A. Li, G. Li and X. Wang, Evaluation of iron-containing aluminophosphate molecular sieve catalysts prepared by different methods for phenol hydroxylation, *Catal. Lett.*, 2013, **143**, 657–665.

2 Y. Wang, Y. Zhou, M. He, Q. He and Y. Zhong, Fe-doped mesoporous alumina: Facile one-pot synthesis, modified surface-acidity and its enhanced catalytic performance in phenol hydroxylation, *Catal. Lett.*, 2020, **150**, 2273–2282.

3 A.D. Salazar-Aguilar, G. Vega, J.A. Casas, S.M. Vega-Díaz, F. Tristan, D. Meneses-Rodríguez, M. Belmonte and A. Quintanilla, Direct hydroxylation of phenol to dihydroxybenzenes by H_2O_2 and Fe-based metal-organic framework catalyst at room temperature, *Catalysts*, 2020, **10**, 172.

4 W.H. Shearon, L.G. Davy and H. von Bramer, Hydroquinone manufacture, *Ind. Eng. Chem.*, 1952, **44**, 1730–1735.

5 Y. Zhao, G. He, W. Dai and H. Chen, High catalytic activity in the phenol hydroxylation of magnetically separable $CuFe_2O_4$–reduced graphene oxide, *Ind. Eng. Chem. Res.*, 2014, **53**, 12566–12574.

6 G. Shi, Y. Bao, B. Chen and J. Xu, Phenol hydroxylation over cubic/monoclinic mixed phase CuO nanoparticles prepared by chemical vapor deposition, *React. Kinet. Mech. Cat.*, 2017, **122**, 289–303.

7 S. Yang, G. Liang, A. Gu and H. Mao, Synthesis of mesoporous iron-incorporated silica-pillared clay and catalytic performance for phenol hydroxylation, *Appl. Surf. Sci.*, 2013, **285**, 721–726.

8 Z. Diao, L. Cheng, W. Guo, X. Hou, P. Zheng and Q. Zhou, Fabrication and catalytic performance of meso-ZSM-5 zeolite encapsulated ferric oxide nanoparticles for phenol hydroxylation, *Front. Chem. Sci. Eng.*, 2021, **15**, 643–653.

9 A.D. Salazar-Aguilar, A. Quintanilla, P. López, C. Martínez, S.M. Vega-Díaz, J.A. Casas, P. Miranzo, M.I. Osendi and M. Belmonte, 3D-printed Fe/γ-Al_2O_3 monoliths from MOF-based boehmite inks for the catalytic hydroxylation of phenol, *ACS Appl. Mater. Interfaces*, 2022, **14**, 920–932.

10 K.M. Parida, S. Singha and P.C. Sahoo, Anchoring of Fe(III)salicylamide onto MCM-41 for catalytic hydroxylation of phenol in aqueous medium using hydrogen peroxide as oxidant, *Catal. Lett.*, 2010, **136**, 155–163.

11 A. Boro and A.K. Talukdar, Phenol hydroxylation over Fe and Co-loaded mesoporous MCM-48, *J. Porous Mater.*, 2019, **26**, 1185–1196.

12 B.-L. Xiang, L. Fu, Y. Li and Y. Liu, Preparation of Fe(II)/MOF-5 catalyst for highly selective catalytic hydroxylation of phenol by equivalent loading at room temperature, *J. Chem.*, 2019, **2019**, 1–10.

13 P. Zhang, X. Sheng, X. Chen, Z. Fang, J. Jiang, M. Wang, F. Li, L. Fan, Y. Ren, B. Zhang, B.J.J. Timmer, M.S.G. Ahlquist and L. Sun, Paired electrocatalytic oxygenation and hydrogenation of organic substrates with water as the oxygen and hydrogen source, *Angew. Chem. Int. Ed.*, 2019, **58**, 9155–9159.

14 Z. Li, C. Liu, W. Geng, J. Dong, Y. Chi and C. Hu, Electrocatalytic ethylbenzene valorization using a polyoxometalate@covalent triazine framework with water as the oxygen source, *Chem. Commun.*, 2021, **57**, 7430–7433.

15 Y. Sun, H. Shin, F. Wang, B. Tian, C.-W. Chiang, S. Liu, X. Li, Y. Wang, L. Tang, W.A. Goddard and M. Ding, Highly selective electrocatalytic oxidation of amines to nitriles assisted by water oxidation on metal-doped α-$Ni(OH)_2$, *J. Am. Chem. Soc.*, 2022, **144**, 15185–15192.

16 M. Gong, C. Cao and Q.-L. Zhu, Paired electrosynthesis design strategy for sustainable CO_2 conversion and product upgrading, *EnergyChem*, 2023, **5**, 100111.

17 R. Wu, Q. Meng, J. Yan, H. Liu, Q. Zhu, L. Zheng, J. Zhang and B. Han, Electrochemical strategy for the simultaneous production of cyclohexanone and benzoquinone by the reaction of phenol and water, *J. Am. Chem. Soc.*, 2022, **144**, 1556–1571.

18 W. Xu, Y. Sun, N. Li, W. Liu and Z.C. Zhang, Copper and cobalt Co-catalyzed selective electrooxidation of phenol to *p*-benzoquinone under mild conditions, *ChemElectroChem*, 2023, **10**, e202300187.

19 S. Abaci, U. Tamer, K. Pekmez and A. Yildiz, Performance of different crystal structures of PbO_2 on electrochemical degradation of phenol in aqueous solution, *Appl. Surf. Sci.*, 2005, **240**, 112–119.

20 Y. Wang, B. Gu and W. Xu, Electro-catalytic degradation of phenol on several metal-oxide anodes, *J. Hazard. Mater.*, 2009, **162**, 1159–1164.

21 L. Suhadolnik, D. Lašič Jurković, B. Likozar, M. Bele, S. Drev and M. Čeh, Structured titanium oxynitride (TiO_xN_y) nanotube arrays for a continuous electrocatalytic phenol-degradation process: Synthesis, characterization, mechanisms and the chemical reaction micro-kinetics, *Appl. Catal. B Environ.*, 2019, **257**, 117894.

22 S. Chen, X. Chu, L. Wu, J.S. Foord, J. Hu, H. Hou and J. Yang, Three-dimensional PbO_2-modified carbon felt electrode for

efficient electrocatalytic oxidation of phenol characterized with in situ ATR-FTIR, *J. Phys. Chem. C*, 2022, **126**, 912–921.
23 B. Pierożyński, G. Piotrowska and T. Mikołajczyk, Kinetics of electrooxidation of phenol on polycrystalline platinum, *Pol. J. Chem. Technol.*, 2015, **17**, 126–130.
24 G. Arslan, B. Yazici and M. Erbil, The effect of pH, temperature and concentration on electrooxidation of phenol, *J. Hazard. Mater.*, 2005, **124**, 37–43.
25 M.D. Baravkar and B.L.V. Prasad, Selective electro-oxidation of phenol to 1,4-hydroquinone employing carbonaceous electrodes: surface modification is the key, *New J. Chem.*, 2022, **46**, 2518–2525.
26 V.M. Vasconcelos, G.O.S. Santos, K.I.B. Eguiluz, G.R. Salazar-Banda and I. De Fatima Gimenez, Recent advances on modified reticulated vitreous carbon for water and wastewater treatment-a mini-review, *Chemosphere*, 2022, **286**, 131573.
27 G. Li, Y. Xu, H. Pan, X. Xie, R. Chen, D. Wu and L. Wang, A bimetallic synergistic effect on the atomic scale of defect-enriched NiV-layered double hydroxide nanosheets for electrochemical phenol hydroxylation, *J. Mater. Chem. A*, 2022, **10**, 6748–6761.
28 Q. Zhang, C. Cao, S. Zhou, W. Wei, X. Chen, R. Xu, X.-T. Wu and Q.-L. Zhu, Bifunctional Oxygen-Defect Bismuth Catalyst toward Concerted Production of H_2O_2 with over 150% Cell Faradaic Efficiency in Continuously Flowing Paired-Electrosynthesis System, *Adv. Mater.,* 2024, **36**, 2408341.
29 Q. Li, D.-D. Ma, W.-B. Wei, S.-G. Han, L. Zheng and Q.-L. Zhu, Value-added Cascade Synthesis Mediated by Paired-Electrolysis Using an Ultrathin Microenvironment-Inbuilt Metalized Covalent Organic Framework Heterojunction, *Adv. Energy Mater.,* 2024, **14**, 2401314.
30 C. Zhu, H. Yue, P. Nikolaienko and M. Rueping, Merging electrolysis and nickel catalysis in redox neutral cross-coupling reactions: Experiment and computation for electrochemically induced C-P and C-Se bonds formation, *CCS Chem.*, 2020, **2**, 179–190.
31 L. Liu, Y. He, Q. Li, C. Cao, M. Huang, D.-D. Ma, X.-T. Wu and Q.-L. Zhu, Self-supported bimetallic array superstructures for high-performance coupling electrosynthesis of formate and adipate, *Exploration*, 2024, **4**, 20230043.
32 X. Li, S.-G. Han, W. Wu, K. Zhang, B. Chen, S.-H. Zhou, D.-D. Ma, W. Wei, X.-T. Wu, R. Zou and Q.-L. Zhu, Convergent paired electrosynthesis of dimethyl carbonate from carbon dioxide enabled by designing the superstructure of axial oxygen coordinated nickel single-atom catalysts, *Energy Environ. Sci.*, 2023, **16**, 502–512.
33 S. Ito, R. Katayama, A. Kunai and K. Sasaki, A novel paired electrosynthesis of p-benzoquinone and hydroquinone from benzene, *Tetrahedron Lett.*, 1989, **30**, 205–206.
34 X. Zhang, Y. Zhu, W. Ahmed and D. Niu, Efficiently Paired Electrosynthesis of Hydroquinone from Phenol by Refreshing the Passivated Pb Anode, *ChemistrySelect*, 2023, **8**, e202301617.
35 N. Sbei, T. Hardwick and N. Ahmed, Green chemistry: Electrochemical organic transformations via paired electrolysis, *ACS Sustain. Chem. Eng.*, 2021, **9**, 6148–6169.
36 L. Muchez, D.E. De Vos and M. Kim, Sacrificial anode-free electrosynthesis of α-hydroxy acids via electrocatalytic coupling of carbon dioxide to aromatic alcohols, *ACS Sustain. Chem. Eng.*, 2019, **7**, 15860–15864.
37 L. Bao, R. Xiong and G. Wei, Electrochemical polymerization of phenol on 304 stainless steel anodes and subsequent coating structure analysis, *Electrochimica Acta*, 2010, **55**, 4030–4038.
38 M. Ferreira, H. Varela, R.M. Torresi and G. Tremiliosi-Filho, Electrode passivation caused by polymerization of different phenolic compounds, *Electrochimica Acta*, 2006, **52**, 434–442.
39 X. Wang, L. Wang, D. Wu, D. Yuan, H. Ge and X. Wu, PbO_2 materials for electrochemical environmental engineering: A review on synthesis and applications, *Sci. Total Environ.*, 2023, **855**, 158880.
40 I. Yahiaoui, F. Aissani-Benissad, K. Madi, N. Benmehdi, F. Fourcade and A. Amrane, Electrochemical pre-treatment combined with biological treatment for the degradation of methylene blue dye: Pb/PbO_2 electrode and modeling-optimization through central composite design, *Ind. Eng. Chem. Res.*, 2013, **52**, 14743–14751.
41 A. Rahmani, A. Seid-mohammadi, M. Leili, A. Shabanloo, A. Ansari, S. Alizadeh and D. Nematollahi, Electrocatalytic degradation of diuron herbicide using three-dimensional carbon felt/β-PbO_2 anode as a highly porous electrode: Influencing factors and degradation mechanisms, *Chemosphere*, 2021, **276**, 130141.
42 L. Burgio, R.J.H. Clark and S. Firth, Raman spectroscopy as a means for the identification of plattnerite (PbO_2), of lead pigments and of their degradation products, *The Analyst*, 2001, **126**, 222–227.
43 I. Costantini, P.P. Lottici, D. Bersani, D. Pontiroli, A. Casoli, K. Castro and J.M. Madariaga, Darkening of lead- and iron-based pigments on late gothic italian wall paintings: Energy dispersive X-ray fluorescence, μ-Raman, and powder X-ray diffraction analyses for diagnosis: Presence of β-PbO_2 (plattnerite) and α-PbO_2 (scrutinyite), *J. Raman Spectrosc.*, 2020, **51**, 680–692.
44 L. Wu, C. Zhang, Y. Sun, Y. Wang, B. Lian, Y. Chen, Y. Tu and T.D. Waite, Cu-mediated optimization of PbO_2 anodes for electrochemical treatment of electroless nickel plating wastewater, *Chem. Eng. J.*, 2022, **450**, 138188.
45 W. Jiang, S. Wang, J. Liu, H. Zheng, Y. Gu, W. Li, H. Shi, S. Li, X. Zhong and J. Wang, Lattice oxygen of PbO_2 induces crystal facet dependent electrochemical ozone production, *J. Mater. Chem. A*, 2021, **9**, 9010–9017.
46 J. Feng, Q. Tao, H. Lan, Y. Xia and Q. Dai, Electrochemical oxidation of sulfamethoxazole by nitrogen-doped carbon nanosheets composite PbO_2 electrode: Kinetics and mechanism, *Chemosphere*, 2022, **286**, 131610.
47 S. Abaci, U. Tamer, K. Pekmez and A. Yildiz, Electrosynthesis of benzoquinone from phenol on α and β surfaces of PbO_2, *Electrochimica Acta*, 2005, **50**,3655–3659.
48 J. Cai, M. Zhou, Y. Pan, X. Du and X. Lu, Extremely efficient electrochemical degradation of organic pollutants with co-generation of hydroxyl and sulfate radicals on Blue-TiO_2 nanotubes anode, *Appl. Catal. B Environ.*, 2019, **257**, 117902.
49 J. Cho, B. Kim, S. Venkateshalu, D.Y. Chung, K. Lee and S.-I. Choi, Electrochemically activatable liquid organic hydrogen carriers and their applications, *J. Am. Chem. Soc.*, 2023, **145**, 16951–16965.
50 J. Huang, B. Pan, W. Duan, X. Wei, R.S. Assary, L. Su, F.R. Brushett, L. Cheng, C. Liao, M.S. Ferrandon, W. Wang, Z. Zhang, A.K. Burrell, L.A. Curtiss, I.A. Shkrob, J.S. Moore and L. Zhang, The lightest organic radical cation for charge storage in redox flow batteries, *Sci. Rep.*, 2016, **6**, 32102.
51 A. Dargahi, D. Nematollahi, G. Asgari, R. Shokoohi, A. Ansari and M.R. Samarghandi, Electrodegradation of 2,4-dichlorophenoxyacetic acid herbicide from aqueous solution using three-dimensional electrode reactor with G/β-PbO_2 anode: Taguchi optimization and degradation mechanism determination, *RSC Adv.*, 2018, **8**, 39256–39268.

View Article Online
DOI: 10.1039/D4IM00067F

The data supporting this article have been included as part of the Supplementary Information.